

Passive Islanding Detection Using Inverter Nonlinear Effects

David Díaz Reigosa, *Member, IEEE*, Fernando Briz, *Senior Member, IEEE*, Cristian Blanco Charro, *Member, IEEE*, and Juan M. Guerrero, *Member, IEEE*

Abstract—This paper analyzes the use of the voltage distortions in pulse width modulation voltage-source inverters caused by the inverter switching for islanding detection purposes. The nonideal characteristics of the inverters, mainly due to the dead time needed to have safe commutations, produce fundamental frequency-dependent harmonics (–5th, 7th, ...) in the output voltage. These harmonic order are, in principle, an unwanted effect, as they reduce the power quality. However, they can potentially be used for islanding detection purposes. The physical principles of the method would be the same as for high-frequency signal injection methods that have already been proposed, but without the need of injecting a high-frequency signal, behaving, therefore, as a passive islanding detection technique.

Index Terms—Dead time, distributed generation, grid impedance estimation, passive islanding detection, power system monitoring.

I. INTRODUCTION

DISTRIBUTED POWER GENERATION (DPG) architectures are a useful mechanism to decrease the transmission losses as well as emissions. Generally speaking, DPG units can be based on renewable and nonrenewable energy resources. One of the most versatile ways to introduce the DPG into the electrical network is throughout the use of microgrids [1], which can be understood as small-scale versions of the classical large centralized electric distribution system.

The connection of microgrids and/or distributed energy resources into the utility grid is regulated by local, regional, and national authorities, while standardizing institutions (e.g., IEEE or IEC) publish standards and recommendations for connecting distributed energy resources into electric power systems [2]–[9]. In every case, the system must have the ability to detect if the DPG unit is connected or disconnected from the utility grid: this is normally referred as islanding detection [10]–[18]. IEEE-1547 [2], UL-1741 [3], IEC-62116 [4], AS-4777 [5], and IEEE-929 [6] are examples of islanding standards.

Manuscript received March 4, 2016; revised June 13, 2016 and November 1, 2016; accepted December 19, 2016. Date of publication January 20, 2017; date of current version June 23, 2017. Recommended for publication by Associate Editor Y. Xue.

The authors are with the Department of Electrical, Computer and System Engineering, University of Oviedo, 33204 Gijón, Spain (e-mail: diaz david@uniovi.es; fernando@isa.uniovi.es; blancocristian@uniovi.es; guerrero@uniovi.es).

Color versions of one or more of the figures in this paper are available online at <http://ieeexplore.ieee.org>.

Digital Object Identifier 10.1109/TPEL.2016.2646751

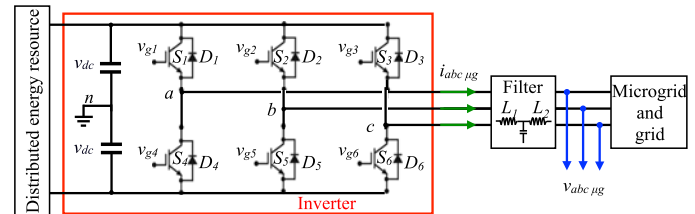


Fig. 1. Simplified distributed energy resource connection to the utility grid/microgrid using a VSI.

Islanding detection methods can be classified into three major groups: passive [10], [11], communication-based [12], and active methods [10]–[18], [33], [35]–[38]. Passive islanding detection techniques detect changes in a grid variable (such as magnitude, frequency, or phase of the point of common coupling (PCC) voltage). These methods are grid friendly, as they do not produce any disturbance in the grid. However, they usually have a large nondetection zone (NDZ), especially when the power mismatch between the power generated by the DPG unit and the power imported from the grid is relatively small. Communication-based methods exchange some information between the grid and the DPGs, requiring, therefore, a communication infrastructure, which results in additional investments. These methods do not have an NDZ unless the communication channel is unavailable [12]. Finally, active islanding detection methods inject a disturbing signal into the grid, the islanding condition being detected by the system response to such a signal [10]–[13]. These methods present a low NDZ [10]–[13], but they have a negative impact on the grid power quality. In addition, the implementation of active methods in a multi-inverter scenario can be problematic due to the interference that can occur between inverters. Strategies to prevent this from happening have been proposed [12], [13].

It is possible to use voltage harmonics that are naturally produced during the normal operation of electronic power converters for islanding detection purposes. Distributed energy resources are usually connected to the main grid/microgrid by means of a three-phase pulse width modulation (PWM) voltage-source inverters (VSIs) [12], [13] (see Fig. 1). VSIs produce a distortion of the output voltage with respect to the commanded voltage, mainly due to the blanking time (dead time) needed for safe commutation of the inverter legs [19]–[24], the turn-on and turn-off times, as well as the voltage drop across the diodes and

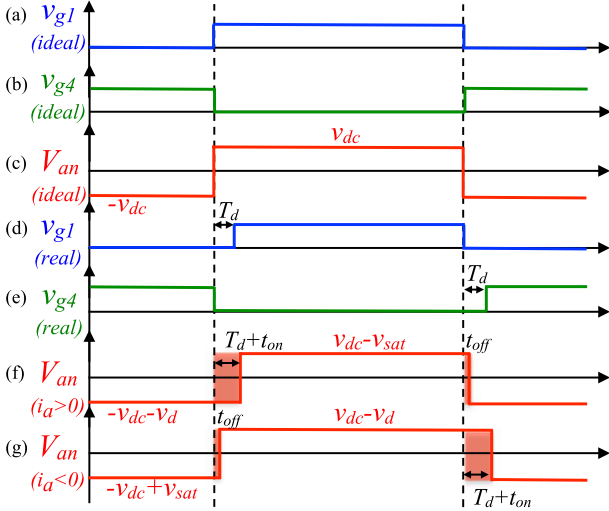


Fig. 2. (a)–(c) Gate signals for switches S1, (a), and S4, (c), and output voltage when no dead time is considered. (d)–(g) Gate signals for switches S1, (d), and S4, (e), when the dead time is inserted. Output voltage when the output current is positive (f) and negative (g).

power switches. Among the aforementioned effects, the dead time is normally the most relevant. The resulting output voltage distortion in this case is known to depend on the inverter current polarity [22], [23], with the -5th , 7th . . . harmonic order of the fundamental frequency appearing in the voltage frequency spectrum [19], [21]. Note that the inverter is connected to the grid via an *LCL* filter, which acts to reduce switching-frequency-related harmonics entering the grid: it usually has a corner frequency higher than the frequency of the harmonics considered here, but will have a small attenuating influence on them.

This paper proposes a new passive islanding detection technique that uses the inverter's nonideal behavior to estimate the grid high-frequency impedance. Since no test signal needs to be injected, there is no adverse impact on the power quality (total harmonic distortion—THD), which is a drawback of active islanding detection methods [12], [13], [10]–[18], [35]–[38]. On the other hand, the method shares the reduced NDZ of active islanding detection methods. Consequently, it combines advantages of both active and passive islanding detection methods.

This paper is organized as follows. The analysis of the effects due to the dead time in PWM inverters is presented in Section II. The principles of the proposed islanding detection method are presented in Section III. Section IV contains some implementation issues that must be carefully taken into account, while simulation and experimental results to confirm the viability of the proposed method are finally provided in Sections V–VII.

II. DEAD-TIME EFFECTS IN PWM INVERTERS

Fig. 1 schematically shows the typical scheme of a three-phase PWM-VSI used to connect distributed energy resources to the three-phase utility grid/microgrid. Fig. 2 shows the gate signals for one leg without [subplots (a)–(c)] and with [subplots (d)–(g)] the dead time.

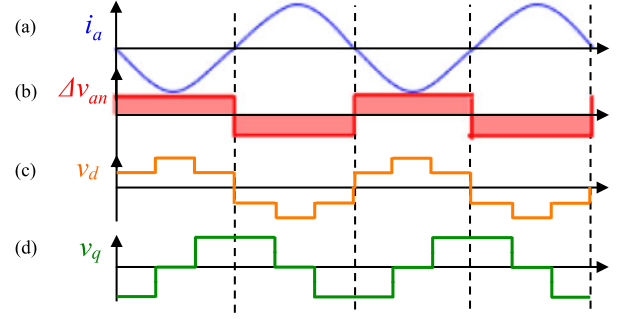


Fig. 3. (a) Phase current. (b) Average voltage error. (c) and (d) *d* and *q* components of the average voltage complex vector.

Fig. 2(a) and (b) shows the ideal gate signals for switches 1 and 4, while Fig. 2(c) shows the ideal output voltage, i.e., when no voltage drop exists across the switches and the ON–OFF transitions of the upper and lower switches occurring simultaneously. In practice, due to the nonzero turn-on and turn-off times, a dead time has to be inserted into every commutation to guarantee that the two switches in a branch (e.g., S1 and S4) do not conduct simultaneously. Fig. 2(d) and (e) shows the real gate signals, after inserting the dead time, when switches S1 and S4 are turned ON and OFF, respectively. When both transistors are turned OFF, one of the freewheeling diodes will conduct, depending on the polarity of the output current. If the current is positive (see Fig. (1)), D4 will be conducting (see Fig. 2(f)), the output voltage being connected to the negative pole of the dc bus. If the current is negative, D1 will conduct and the output voltage will be connected to the positive pole of the of the dc bus. The voltage drops across the switches and diodes as well as the turn-on/off times are also schematically shown in Fig. 2(f) and (g).

The average voltage errors caused by the nonideal behavior of the inverter (turn-on, turn-off, voltage drops, and dead time) during each switching period can be understood from (1) and (2) for the case of the current being positive and negative, respectively [see Fig. 2(f) and (g)], where t_d is the dead time, t_{on} is the turn-on time of the power switch, t_{off} is the turn-off time of the power switch, T_s is the sampling period, V_{dc} is the dc-bus voltage, V_d is the forward voltage drop of the diode, and V_{sat} is the on-state voltage drop across the power switch. Assuming that $V_d \approx V_{sat}$, (1) and (2) can be simplified to (3) and (4) [22].

Fig. 3(a) shows the current for phase *a*, while Fig. 3(b) shows the average voltage error over each switching cycle. The average voltage corresponds to a square wave, which can be expressed using a Fourier series as (5). Taking into account the $2\pi/3$ phase shift between phases in a balanced three-phase system, the average voltage errors for phases *b* and *c* can be expressed as (6) and (7), with *n* being the harmonic order

$$\begin{aligned} \Delta V &= \frac{T_d + t_{on}}{2T_s} (-V_{dc} - V_d) + \frac{t_{off}}{2T_s} (V_{dc} - V_{sat}) \\ &= \frac{-T_d - t_{on} + t_{off}}{2T_s} V_{dc} + \frac{-T_d - t_{on}}{2T_s} V_d + \frac{-t_{off}}{2T_s} V_{sat} \end{aligned} \quad (1)$$

$$\begin{aligned}\Delta V &= \frac{T_d + t_{on}}{2T_s} (V_{dc} + V_d) + \frac{t_{off}}{2T_s} (-V_{dc} + V_{sat}) \\ &= \frac{T_d + t_{on} - t_{off}}{2T_s} V_{dc} + \frac{T_d + t_{on}}{2T_s} V_d + \frac{t_{off}}{2T_s} V_{sat}\end{aligned}\quad (2)$$

$$\Delta V = \frac{-T_d - t_{on} + t_{off}}{2T_s} V_{dc} - \frac{T_d + t_{on} + t_{off}}{2T_s} V_{sat}\quad (3)$$

$$\Delta V = \frac{T_d + t_{on} - t_{off}}{2T_s} V_{dc} + \frac{T_d + t_{on} + t_{off}}{2T_s} V_{sat}\quad (4)$$

$$V_{an} = \frac{4\Delta V}{\pi} \sum_{n=1,5,7,\dots} \frac{1}{n} \sin(n\omega t)\quad (5)$$

$$V_{bn} = \frac{4\Delta V}{\pi} \sum_{n=1,5,7,\dots} \frac{1}{n} \sin\left[n\left(\omega t - \frac{2\pi}{3}\right)\right]\quad (6)$$

$$V_{cn} = \frac{4\Delta V}{\pi} \sum_{n=1,5,7,\dots} \frac{1}{n} \sin\left[n\left(\omega t - \frac{4\pi}{3}\right)\right].\quad (7)$$

Using the transformation from a generic set of three-phase quantities (f_a, f_b, f_c) to dq quantities (8), the resulting voltage vector due to the nonideal behavior of the inverter (8) is obtained, the corresponding d - and q -axis components being shown in Fig. 3(c) and (d), respectively. Voltage and current complex vectors in the following equations and figures are referred to the stationary reference frame. It is noted, however, that other reference frames could be used, in practice, for the implementation of the control and signal processing algorithms described in this paper

$$v_{dq} = \sum_{n=-5,7,-11,13,\dots} V_n e^{j(n\omega_0 t + \theta_n)}\quad (8)$$

$$f_{dq} = f_d + jf_q = \frac{2}{3} \left(f_a + f_b e^{j2\pi/3} + f_c e^{j4\pi/3} \right)\quad (9)$$

$$V_n = \frac{4 \cdot \Delta V}{n\pi}\quad (10)$$

where $\theta = \pi$ when $n < 0$ and $\theta = -\pi$ when $n > 0$, ω_0 is the grid/microgrid frequency, and the magnitude of the harmonic voltage V_n is given by (10).

It is concluded from (5)–(8) that the inverter nonideal behavior produces harmonics having orders of $-5, 7, \dots$, with the corresponding harmonic magnitude being inversely proportional to the harmonic order (10) [27] (see Fig. 4).

Figs. 5 and 6 show the experimentally measured frequency spectrum of the output voltage and current of a VSI, both for the case of island and grid-connected operation (the experimental setup is shown in Fig. 16, its parameters being shown in Table III). An LCL filter was used to connect the VSI to the grid. The current for the case of island operation corresponds, therefore, to the current absorbed by the LCL filter. Harmonics of order -5 and 7 are readily observed in the voltage and current spectrums, their magnitudes being inversely proportional to the harmonic order. It can also be seen that harmonics induced in the resulting current vector due to the nonideal behavior of the inverter are noticeably higher in the grid-connected case compared to the island case. This is due to the lower output

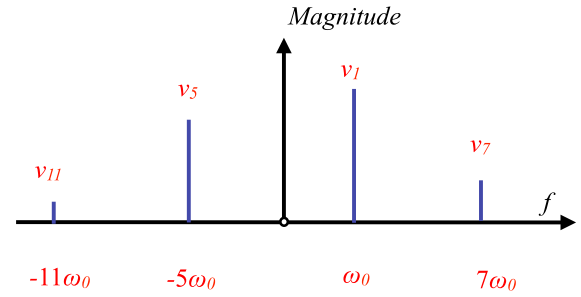


Fig. 4. Schematic representation of the complex vector spectrum of the output voltage vector showing the harmonics due to the nonideal behavior of the inverter, v_{dq} .

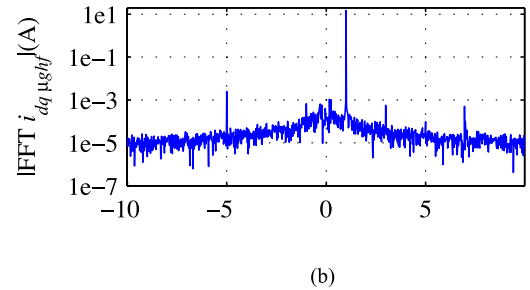
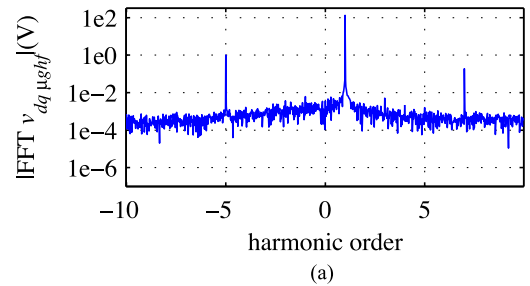


Fig. 5. (a) Voltage complex vector ($v_{dq\mu g}$) and (b) current complex vector ($i_{dq\mu g}$) spectrums in the island mode. The fundamental frequency is 50 Hz, with a dead time of $3\mu s$ and a switching frequency of 10 kHz.

impedance for the case of the grid-connected mode. It is also noted that the resulting higher order harmonics at the output voltage of the LCL filter are smaller for the grid-connected case with respect to the island case. This is due to the increased voltage drop across the filter due to the larger harmonic currents.

III. ISLANDING DETECTION USING HARMONICS DUE TO THE INVERTER SWITCHING

The harmonics due to nonideal behavior of the VSI (8) can be modeled as (11). Every harmonic in the output voltage (v_{dqn} ; see Fig. 7) will produce a harmonic in the inverter current at the same frequency ($i_{dq n}$; see Fig. 7). The resulting harmonic component at the output of the LCL filter (12) can be obtained by applying Kirchhoff's voltage law to the output LCL filter, as

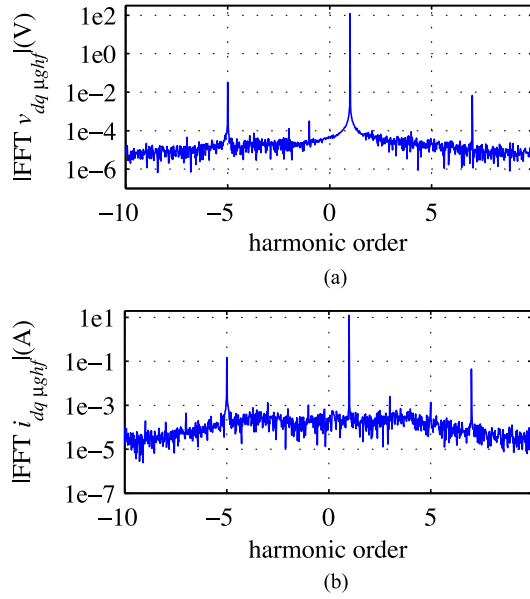


Fig. 6. (a) Voltage complex vector ($v_{dq\mu g}$) and (b) current complex vector ($i_{dq\mu g}$) spectrums in the grid-connected mode. The operating conditions are the same as in Fig. 5.

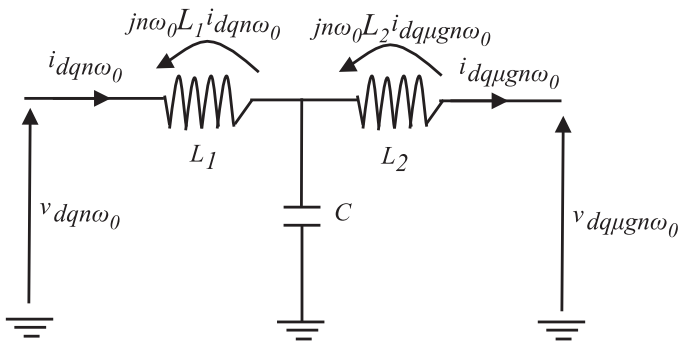


Fig. 7. Single-phase representation of the output LCL filter voltages and currents.

shown in Fig. 7

$$v_{dq\mu n} = V_n e^{jn\omega_0 t} \quad (11)$$

$$i_{dq\mu gn} = \frac{v_{dq\mu n} - v_{dq\mu gn} - jn\omega_0 L_1 i_{dq\mu n}}{jn\omega_0 L_2} \quad (12)$$

$$Z_{dq\mu gn} = \frac{v_{dq\mu gn}}{i_{dq\mu gn}} \quad (13)$$

where $v_{dq\mu gn}$ is the magnitude of the resulting voltage harmonic at the filter output (see Fig. 7), L_1 is the inverter-side inductance, and L_2 is the grid/microgrid-side inductance. The high-frequency impedance (13) is obtained from the voltage and current harmonics due to the nonideal behavior of the inverter. Variations of the high-frequency impedance will be used to detect islanding [12], [13], [33], [36].

In principle, any of the high-order harmonics due to the nonideal behavior of the inverter could be potentially used for islanding detection purposes. However, lower order harmonics

will provide a larger signal-to-noise ratio, improving the accuracy of the method. This is due both to the decrease of the harmonic voltage magnitude with the harmonic order (10) and to the increase of the impedance with the harmonic order due to its inductive nature. The maximum harmonic order might also be limited by the interaction between the injected harmonics, the LCL filter resonance frequency, and the grid resonance frequency [12]. It is concluded that the -5 th and the 7 th harmonic order are the preferred candidates for the implementation of the method.

In the following subsections, two different strategies for the implementation of the proposed methods are discussed, namely the open-loop mode and the current cancellation mode.

A. Open-Loop Mode

In this mode of operation, no mechanism is implemented to compensate the effects due to the nonideal behavior of the inverter. The harmonics in the inverter output voltage [$v_{dq\mu n}$ in Fig. 7 and (11)] and current [$i_{dq\mu n}$ in Fig. 7 and (12)] are used to estimate the high-frequency impedance (13). Islanding is detected from the changes in the high-frequency impedance magnitude and phase.

Fig. 8 shows the block diagram of the signal processing used for islanding detection using this mode of operation, including the current control of the inverter as well as the filtering. A voltage control loop and higher level control functionalities are not included in the diagram, since they do not interfere with the proposed islanding detection method. Two bandpass filters (BPF1 and BPF2; see Fig. 8), tuned at the frequency of the harmonic used for islanding detection, are used to isolate the corresponding voltage and current harmonic components. It is finally noted from Fig. 8 that no explicit high-frequency signal injection exists, contrary to active islanding detection methods reported in [12] and [39].

Since the proposed method is based on the high-frequency impedance variation between island and grid-connected operating modes, an NDZ can occur when the difference between the microgrid and the grid high-frequency impedance is small (e.g., below the limits established by the standards [7]–[9]) or the voltage difference between the inverter output and the PCC. It is noted, however, that these limitations are shared by all islanding detection methods based on the measurement of impedance variation. It is also noted that since the method is based on the microgrid/grid high-frequency impedance variation, it will be sensitive to the length/impedance of the line between the inverter and the PCC. An analysis of this issue, including remedial measurements, has already been presented in [33].

Finally, although the proposed method must be considered as passive, since no disturbing signal is being injected, its NDZ matches with that of active methods [10]–[18], [33], [36]. The NDZ in passive methods is typically defined as a region of active and reactive fundamental power mismatch where the islanding condition cannot be detected [11]; however, this definition cannot be applied in this case, as the proposed method is not based on a power mismatch but on the high-frequency impedance variation.

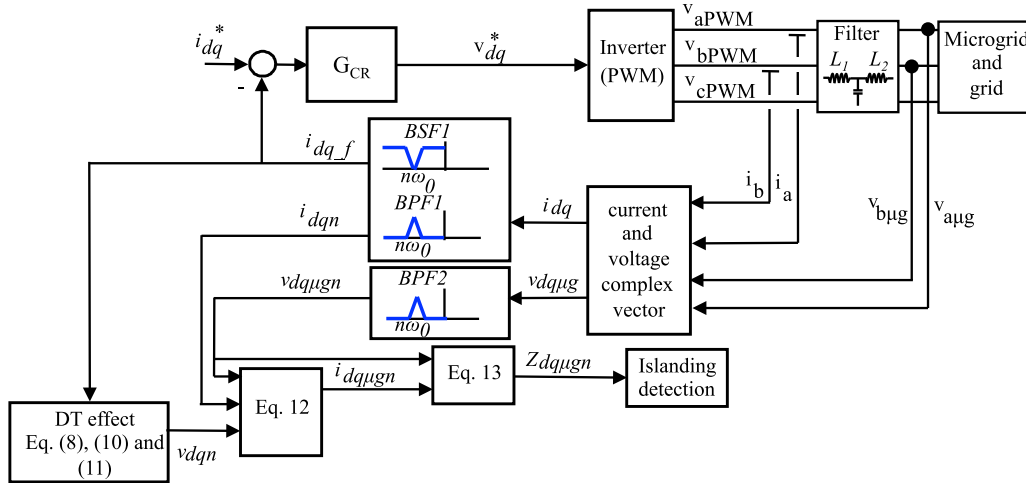


Fig. 8. Signal processing for islanding detection using the high-frequency impedance variation using an open-loop implementation.

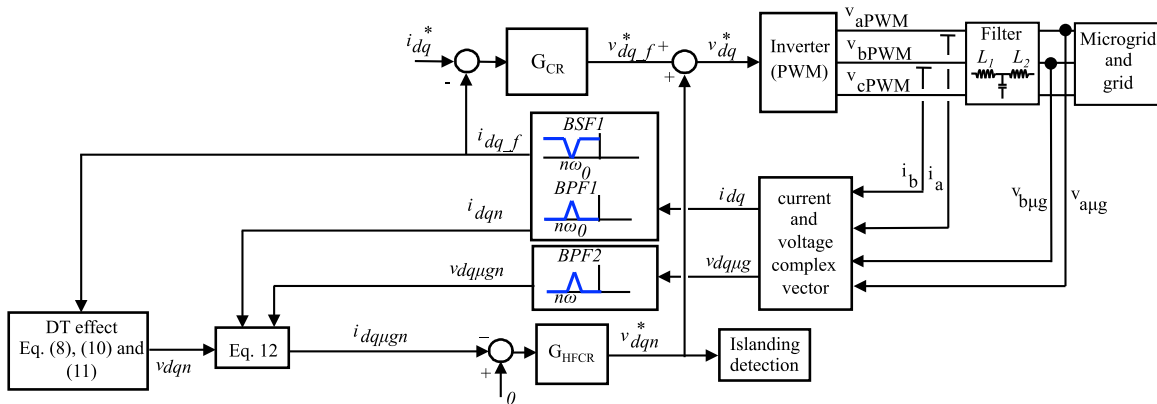


Fig. 9. Signal processing for islanding detection for the current cancellation mode.

B. Current Cancellation Mode

An alternative implementation of the method named current cancellation mode is shown in Fig. 9. In this strategy, a PI regulator (G_{HFCR} in Fig. 9) in a reference frame synchronous with the harmonic used for islanding detection, $n\omega_0$, is used to eliminate the harmonic from the inverter output current. The output of the harmonic current regulator ($v_{dq_n}^*$ in Fig. 9) corresponds to the harmonic voltage needed to cancel the harmonic current. The magnitude of this voltage can be used for islanding detection purposes [13]. As for the open-loop mode, the voltage control loop and higher level control functionalities are not shown in Fig. 9, as they do not affect to the implementation of the method.

The threshold for islanding detection, both for open-loop and current cancellation modes, is highly influenced by the microgrid structure and parameters (LCL filters, transition lines, loads, inverters, and nonlinear loads (NLLs)). There is, therefore, no limit for the number of potential configurations. It is noted that the same problem exists for all islanding detection methods based on the injection of a harmonic/high-frequency signal. This issue has been not investigated in the literature by analytical procedures, being the object of ongoing research.

IV. IMPLEMENTATION ISSUES

There are five aspects that can be especially relevant for the implementation of the proposed method:

- 1) dead time used in the inverter;
- 2) the risk of interference with NLLs;
- 3) grid voltage harmonics;
- 4) the effects of dead-time compensation strategies;
- 5) interference among inverters operating nearby.

All these issues are discussed in this section.

A. Dead Time Used in the Inverter

The proposed method uses the variations of the high-frequency impedance to detect changes between grid-connected and island modes. Consequently, its operation should be independent, in principle, of the dead time used in the VSI. However, this is not totally true in practice. The selection of the dead time will affect the signal-to-noise ratio: the larger the dead time, the larger will be the magnitude of the induced voltage distortion and consequently the resulting harmonic currents, therefore improving the signal-to-noise ratio of the estimated impedance.

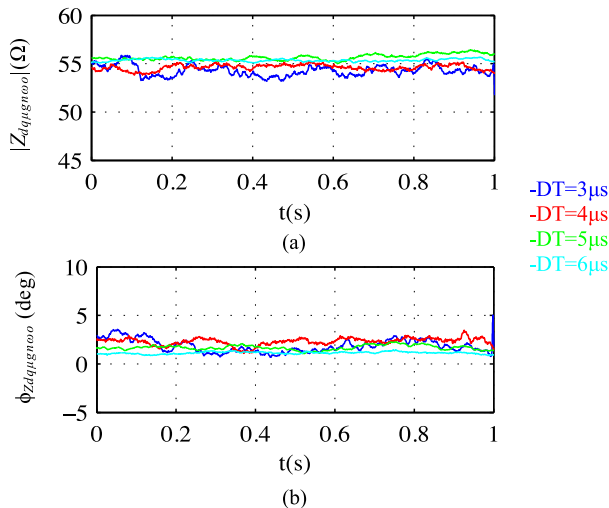


Fig. 10. Experimental results. (a) Magnitude and (b) phase of the estimated high-frequency impedance for different values of the dead times.

TABLE I
SIMULATION PARAMETERS: SINGLE-INVERTER OPERATION

Grid	380 V, 50 Hz, $S_{cc} = 15$ MVA
Inverter	380 V, 10 kHz.
RLC Load	$R = 43 \Omega$, $L = 136.9$ mH, $C = 74 \mu\text{F}$
RLC Load Quality factor [2]	1
Simulation step	$1e-7$ s
Dead time	$5 \mu\text{s}$
BPF1, BPF2, and BSF1 bandwidth	25 Hz
G_{CR}	$K_p = 10$; $K_i = 95$
G_{HFCR}	$K_p = 15$; $K_{i-} = 200$
LCL filter resonance frequency	575 Hz

For the case of small values of the dead time, a low-pass filter can be used to eliminate noise from the estimated high-frequency impedance.

Fig. 10 shows the estimated high-frequency impedance for values of the dead time ranging from 3 to 6 μs , respectively, which correspond to the minimum and maximum values that can be used in the experimental setup, respectively (the details can be found in Table I and Fig. 11). As expected, the estimated high-frequency impedance (magnitude and phase) is less oscillatory for the case of the larger dead time. Since lower dead times would be preferred from a power quality perspective, there is a compromise, which is required in practice.

B. Risk of Interference With NLLs

NLLs can potentially interfere with the proposed method, as they can produce harmonics at frequencies that coincide with those due to the nonideal behavior of the inverter. The performance of the method in this case can strongly depend on the microgrid structure. To the best of authors' knowledge, detailed analysis of this issue has not been reported in the literature. Although its detailed analysis is beyond the scope of this paper, discussion of the key concepts involved is briefly presented in the following.

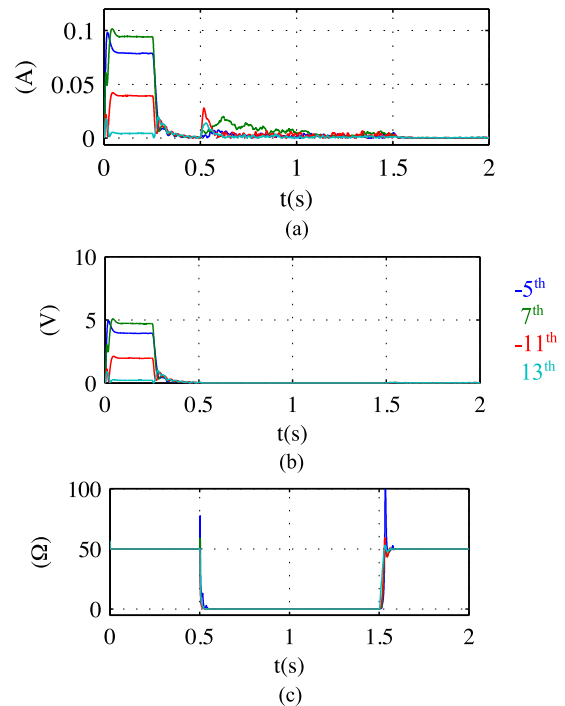


Fig. 11. Simulation results for the dead-time compensation technique shown in [40]. (a) Magnitude of the -5^{th} , 7^{th} , -11^{th} , and 13^{th} current harmonics. (b) Magnitude of the -5^{th} , 7^{th} , -11^{th} , and 13^{th} voltage harmonics. (c) Magnitude of the estimated high-frequency impedance for the -5^{th} , 7^{th} , -11^{th} , and 13^{th} harmonic components. Dead time = 5 μs .

There are two major issues that will influence the performance of high-frequency signal injection based islanding detection methods in the presence of NLLs.

- 1) *Frequency selection*: It can coincide with a characteristic harmonic components of the fundamental frequency (-5 , 7 , 11 , 13 , \dots , i.e., those produced by NLLs) or not; the method proposed in this paper uses a characteristic frequency, as the harmonics due to the dead time in the inverter are of these types.
- 2) *Presence of active power filters (APFs) in the microgrid implementing harmonic current compensation*: It is noted that the presence of APFs implies a multi-inverter scenario.

Use of characteristic harmonics is expected to provide excellent performance when APFs operate in the microgrid. Since the APF supplies the harmonic current consumed by NLLs, the NLL will become invisible to the harmonics induced by the nonlinear behavior of the inverter (no current will flow from the inverter to the NLL), the inverter seeing an infinite impedance at its output. However, when the inverter is grid connected and the APF continues supplying the harmonic current consumed by the NLLs, the high-frequency impedance that the inverter sees at its output will decrease due to the reduced grid impedance magnitude. Therefore, the method proposed in this paper is advantageous in this case, as it uses characteristic harmonics. On the contrary, use of noncharacteristic harmonics would be highly inadvisable when APF operates in the microgrid, as the reaction of the APF to such harmonics is highly

unpredictable, depending on the frequency being used and the configuration of the APF. Both characteristic and noncharacteristic harmonics can potentially provide similar performance when APFs are not used in the microgrid.

C. Effects of Grid Voltage Harmonics

The presence of harmonic components in the grid voltage could decrease the method accuracy, eventually driving the method into the NDZ or even erroneously detecting the islanding condition. Nevertheless, this is not a particular limitation of this method; it is shared by all active islanding techniques based on the injection of a harmonic/high-frequency signal.

The advantage of the proposed technique is that any of the high-order harmonics due to the nonideal behavior of the inverter could be potentially used for islanding detection purposes (i.e., not only -5 th harmonic component). Therefore, harmonic component that are not expected to be present could be used instead of the -5 th.

D. Effects of Dead-Time Compensation Techniques

Inverters commonly implement dead-time compensation techniques [20]–[26], [40]–[48]. The reliability of the proposed technique could be compromised in inverters implementing these techniques. The reliability of the proposed islanding detection technique has been evaluated for the dead-time compensation strategy presented in [40].

Fig. 11 shows the simulation results for the compensation technique presented in [40]. Fig. 11(a) shows the magnitude of the current harmonics (-5 th to 13th), i_{dqgn} (11), while Fig. 11(b) shows the magnitude of the voltage harmonics at the filter output ($v_{dq\mu gn}$; see Fig. 7). The dead-time compensation strategy is activated at $t = 0.25$ s, the inverter is connected to the grid at $t = 0.5$ s and disconnected from the grid at $t = 1.5$ s. It is observed from Fig. 11(a) that the compensation technique compensates the current harmonics ≈ 100 ms after the strategy is being activated. Finally, Fig. 11(c) shows the magnitude of the high-frequency impedance (13) for the harmonic components shown in Fig. 11(a) and (b). It is observed that the islanding condition can be reliably detected even in inverters implementing dead-time compensation techniques.

It is finally noted that dead-time compensation techniques typically do not compensate for all harmonic components due to the nonideal behavior of the inverter [40], [42]–[48]. Although in the paper it is proposed to use the -5 th harmonic component, in principle, any of the high-order harmonics due to the nonideal behavior of the inverter that is not being compensated by the compensation technique could be used for islanding detection purposes. Therefore, as verified in simulation results, the method applicability is not compromised by the implementation of dead-time compensation techniques.

E. Interference Among Inverters Operating Nearby

When multiple inverters using a high-frequency signal for islanding detection operate nearby, synchronization of the high-frequency signal for all the inverters is highly advisable [33].

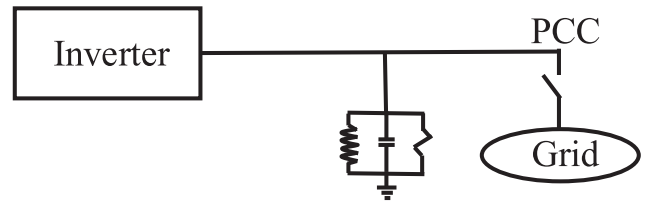


Fig. 12. Simulation scenario for IEEE-1547 islanding detection test conditions.

Otherwise, the circulating currents among the inverters due to differential high-frequency voltages can produce an unwanted interference among inverters. Since the effect of the dead time is related to the zero crossing of the current, inverters operating with the same power angle will be self-synchronized. This would be the case when all the inverters operate with a unit power factor. If the power factor is different for inverters located nearby (e.g., if the inverters are commanded to compensate reactive power), then a differential high-frequency voltage among inverters could occur. This would produce the circulation of high-frequency currents among inverters, therefore reducing the accuracy estimating the high-frequency impedance. Strategies to prevent this to happen have already been analyzed in [13] and [33]; they are not, therefore, discussed in detail in this work. The strategy proposed in [13] can be adopted in this case, where one of the inverters would work in an “open-loop mode” and the remaining inverters would work in a “current cancellation mode.” Inverters using the combined “open-loop mode” and “current cancellation mode” can be directly connected in parallel.

V. SIMULATION RESULTS UNDER IEEE-1547 ISLANDING DETECTION TEST CONDITIONS

The proposed strategy has been evaluated in a single-inverter scenario using the IEEE-1547 islanding detection test conditions. The simulation scenario is shown in Fig. 12, the simulation parameters being given in Table I.

Fig. 13(a) and (b) shows the magnitude and phase of the estimated high-frequency impedance in a transition from island to grid connected ($t = 0.5$ s) and from grid connected to island ($t = 1.5$ s), using the open-loop mode (see Fig. 8). The -5 th harmonic was used for the impedance estimation.

It is observed from Fig. 13 that both the magnitude and phase of the high-frequency impedance could be potentially used for islanding detection. The change of the high-frequency impedance is detected in a few ms, widely meeting the islanding detection requirements (e.g., 1Ω in 2 s for the German standard [7] and 0.5Ω in 5 s for the Swiss and Australian standards [8], [9]).

Fig. 14 shows the harmonic current regulator output voltage when the current cancellation mode shown in Fig. 9 is used, for the same transition as in Fig. 13. Also, in this case, the change of the current regulator output voltage takes a few ms, therefore meeting the islanding detection standards [2]–[9].

To illustrate the differences between the current cancellation mode versus the open-loop mode, Fig. 15 shows the magnitude

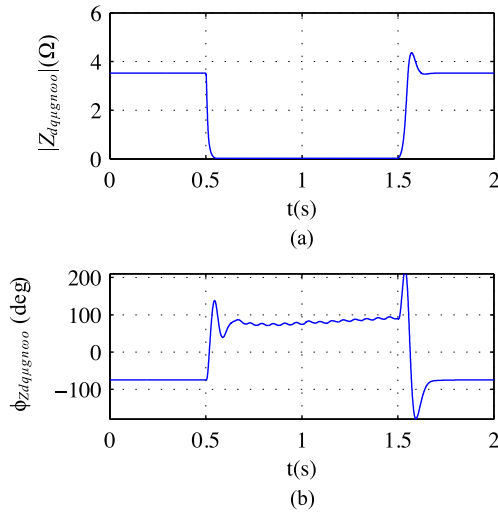


Fig. 13. (a) Magnitude and (b) phase of the estimated high-frequency impedance.

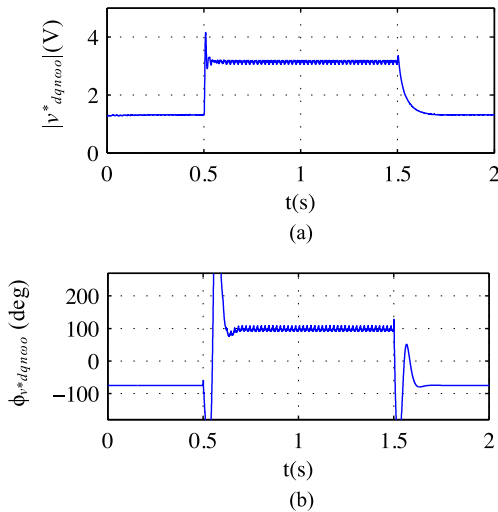


Fig. 14. (a) Magnitude and (b) phase of the harmonic current regulator output voltage.

of the -5 th, 7 th, -11 th, and 13 th harmonics of the current vector in both cases. The current cancellation mode is seen to significantly reduce the -5 th harmonic of the current, therefore improving the THD.

VI. SIMULATION RESULTS FOR PARALLEL-INVERTER OPERATION

The proposed method has been evaluated for the multi-inverter scenario, as shown in Fig. 16. The simulation parameters are shown in Table II. The no-load-sharing strategy was implemented for the converters, while the -5 th harmonic was used for the impedance estimation.

Fig. 17(a) and (b) shows the magnitude and phase of the estimated high-frequency impedance in a transition from island to grid-connected ($t = 0.5$ s) and from grid-connected to island

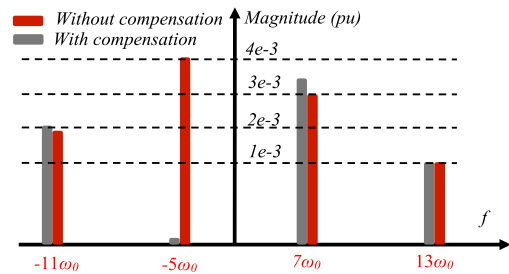


Fig. 15. Harmonics of the current vector with and without compensation of the fifth harmonic implemented.

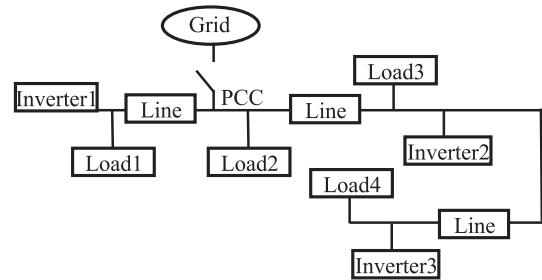


Fig. 16. Multi-inverter simulation scenario.

TABLE II
SIMULATION PARAMETERS: PARALLEL-INVERTER OPERATION

Grid	380 V, 50 Hz, $S_{cc} = 15$ MVA
Inverters 1, 2, and 3	380 V, 10 kHz.
Load1,2,3 and 4	10 kW
Line	11.7 mΩ, 8.68e-4 H
Simulation step	1e-7 s
Dead time	5 μs
BPF1, BPF2, and BSF1 bandwidth	25 Hz
G_{CR}	$K_p = 10; K_i = 95$
G_{HFCR}	$K_p = 15; K_i = 200$
LCL filter resonance frequency	575 Hz

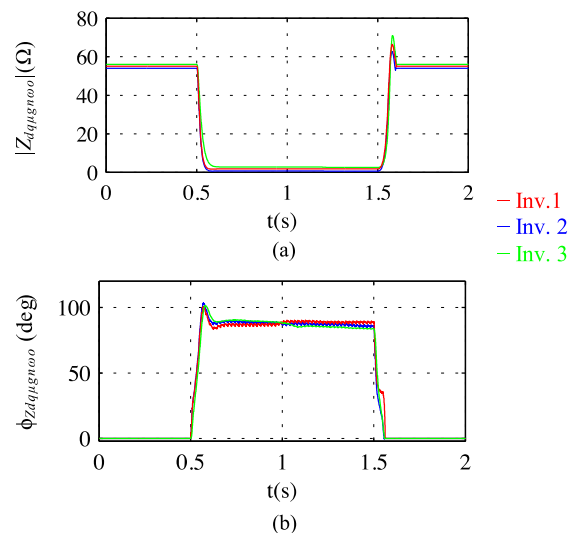


Fig. 17. Simulation results when the inverters operated in the open-loop mode. (a) Magnitude. (b) Phase.

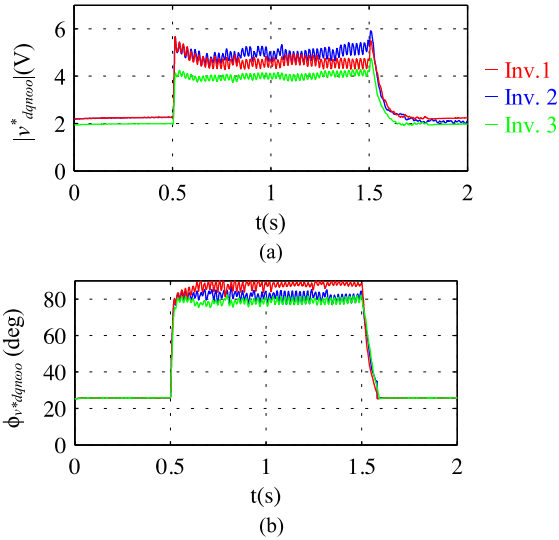


Fig. 18. Simulation results when the inverters operated in the current cancellation mode. (a) Harmonic current regulator output voltage. (b) Phase.

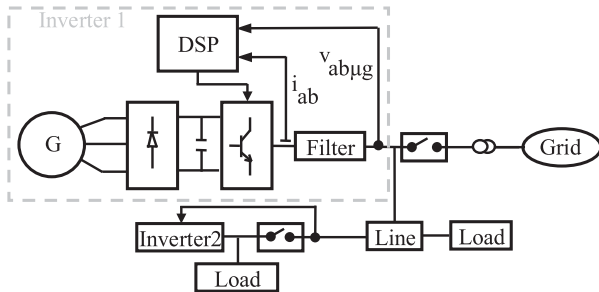


Fig. 19. Experimental setup with two parallel-connected inverters.

($t = 1.5$ s) with the inverter operating in an open-loop mode, the high-frequency impedance being used for islanding detection (see Fig. 8). Minor differences observed in Fig. 17(a) and (b) among inverters 1, 2, and 3 are due to the differences in the corresponding line impedances. It is observed, however, that in all the cases, the transition between the grid-connected and island modes is readily observable.

Fig. 18(a) and (b) shows the response of the method using the current cancellation mode. Changes of the harmonic current regulator output voltage (see Fig. 9) reliably reflect the changes between the grid-connected and island modes.

VII. EXPERIMENTAL RESULTS

Experimental results showing the performance of the proposed method are presented in this section. Only results for the multi-inverter scenario will be provided, as this case is significantly more challenging compared to the single-inverter case. Fig. 19 shows the experimental setup, the main parameters being shown in Table III. The three-phase inverters use Mitsubishi Electric 1200-V, 75-A insulated-gate bipolar transistor modules. The dead time was set to $3 \mu\text{s}$, which is the minimum value allowed by the power modules. The switching frequency was

TABLE III
EXPERIMENTAL SETUP PARAMETERS: PARALLEL-INVERTER OPERATION

Grid ratings	380 V, 50 Hz, $S_{cc} = 2 \text{ MVA}$
Grid harmonic content	5th = 0.195%, 7th = 0.087%, 11th = 0.033%.
Generator	380 V, 10 kHz, 100 kVA.
Inverter 1 and 2 ratings	380 V, 10 kHz, 30 kVA.
Inverter 1 LCL filter parameters	$L = 2.4 \text{ mH}$, $C = 30 \mu\text{F}$
Inverter 2 LCL filter parameters	$L = 1.56 \text{ mH}$, $C = 30 \mu\text{F}$
Load 1 and 2	30 kW
Dead time	$3 \mu\text{s}$
BPF1, BPF2, and BSF1 bandwidth	10 Hz
G_{HFGR}	$K_p = 12.6$; $K_i = 71.5$
G_{CR}	$K_p = 8.4$; $K_i = 60$

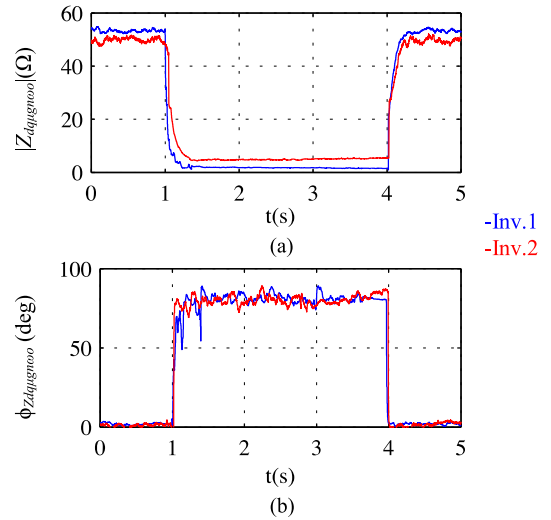


Fig. 20. Experimental results when the inverters operate in the open-loop mode. (a) Magnitude. (b) Phase. Dead time = $3 \mu\text{s}$.

set to 10 kHz. The -5 th harmonic was used for the impedance estimation.

Fig. 20 shows the estimated high-frequency impedance magnitude and phase using the implementation shown in Fig. 8 (open-loop mode), during a transition from island to grid-connected ($t = 1$ s) and from grid connected to island ($t = 4$ s). The estimated high-frequency impedance is available in ≈ 100 ms: this was considered fast enough for island detection (according to [2]–[6]). The experimental results were repeated for many scenarios, and in each case, an identifiable change in impedance indicating a grid-island transition was identified, shown that the technique was repeatable and potentially reliable. The differences between the high-frequency impedance seen by the inverters are related to the different LCL filters, the transmission lines, and the loads connected to the PCC (see Fig. 16).

Fig. 21 shows the harmonic current regulator output voltage using the current cancellation mode (see Fig. 9) for the same transition shown in Fig. 20. Again, it is observed that the change on the current regulator output voltage occurs in a few milliseconds, both the magnitude and phase being potentially useful for islanding detection purposes. The differences among the voltages required to compensate the high-frequency current are due

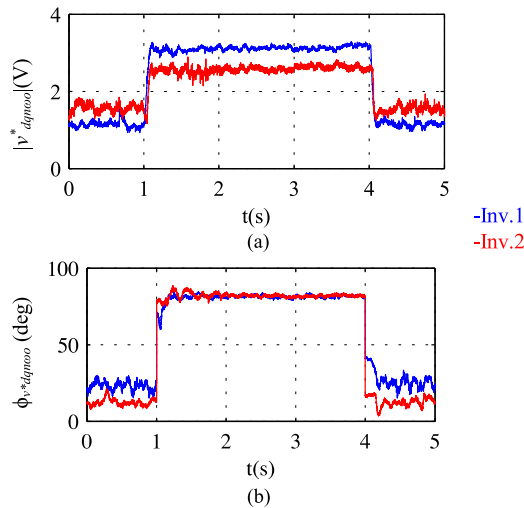


Fig. 21. Experimental results when the inverters operate in the current cancellation mode. (a) Harmonic current regulator output voltage. (b) Phase. Dead time = 3 μ s.

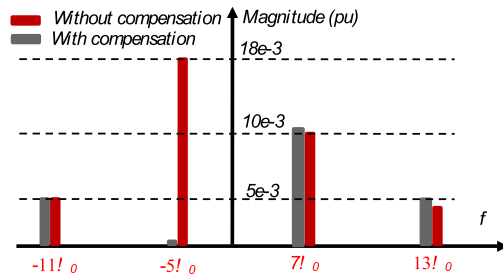


Fig. 22. Experimentally measured harmonics of the current complex vector with and without compensation of the -5 th harmonic implemented at the PCC. Dead time = 3 μ s.

to the different lines impedances (i.e., lines between the inverters and the PCC). In this case, inverter 2 has a transmission line placed between its *LCL* output and the *PCC* (see Fig. 19) that makes smaller the required voltage to compensate its input current. It is finally noted that although the variation of the current PI regulator output (see Fig. 21) between the island and grid-connected modes is small, the signal is very clean, the transition being, therefore, reliably detected.

Finally, Fig. 22 shows the magnitude of the most relevant current harmonics due to the nonideal behavior of the inverter for the open-loop and current cancellation modes, respectively. As expected, the current cancellation mode eliminates the selected component of the harmonic current. It is noted that the current THD at the PCC is $\approx 2.13\%$ in the open-loop mode, reducing to $\approx 1.6\%$ in the current cancellation mode, i.e., when the -5 th harmonic is compensated by the harmonic current regulator (see Fig. 9).

VIII. CONCLUSION

An islanding detection method that uses harmonic components of the fundamental frequency caused by the nonideal behavior of the inverter (mainly the dead time) has been presented

in this paper. The proposed method provides a reduced NDZ, similar to an active islanding detection method. However, since these harmonic components occur naturally and no additional signal needs to be injected, it has no adverse effect on the system power quality. Consequently, it combines the reduced NDZ of active islanding detection methods with the grid-friendly properties of passive islanding detection methods.

Two different implementations, namely the open-loop mode and the current cancellation mode, have been proposed, the second providing better performance in general, as it improves the current THD at PCC and can be used in scenarios with multiple inverters operating in parallel.

Simulations and experimental results have been provided to confirm the viability of the method. Changes between island and grid-connected conditions can be detected in ≈ 100 ms, which is fast enough to meet the islanding detection standards [2]–[9]. Regardless of the relatively small value of the voltage harmonics due to the dead time compared to the values reported in the literature for other high-frequency signal-injection-based methods [12], [13], [10]–[18], [35]–[38], implementation of the method has not required special voltage and current sensors in most of the applications. Finally, the computational requirements of the method are relatively small, meaning that it can be easily integrated into the type of digital signal processors that are currently being used in grid-connected VSIs.

REFERENCES

- [1] R. Lasseter, "MicroGrids," in *Proc. IEEE Power Eng. Soc. Winter Meeting*, New York, NY, USA, Jan. 2002, pp. 305–308.
- [2] *IEEE Standard for Interconnecting Distributed Resources with Electric Power Systems*, IEEE Standard 1547-2003, 2003.
- [3] *UL Standard for Safety for Static Converters and Charge Controllers for Use in Photovoltaic Power Systems*, UL1741, May 7, 1999 (revised Jun. 2001).
- [4] *Testing Procedure of Islanding Prevention Measures for Grid Connected Photovoltaic Power Generation Systems*, IEC 62116, Int. Electrotech. Commission, 2014.
- [5] *Grid Connection of Energy Systems via Inverters Part 3: Grid Protection Requirements*, Australian Standard AS4777, 2005.
- [6] *IEEE Recommended Practice for Utility Interface of Photovoltaic (PV) Systems*, IEEE Standard 929-2000, Apr. 2000.
- [7] *Automatic Disconnection Device Between a Generator and the Low-Voltage Grid*, DIN-VDE Standard 0126-1-1, 2005.
- [8] *Photovoltaische Energieerzeugungsanlagen—Sicherheitsanforderungen (Photovoltaic power generating systems—Safety requirements)*, ÖVE/Önorm E 2750, 2004.
- [9] *VSE Sonderdruck Abschnitt 12 'Werkvorschriften über die Erstellung von elektr. Installation' Elektrische Energieerzeugungsanlagen Completes*, VSE 2.8d-95, 1997.
- [10] A. Timbus, A. Oudalov, and C. N. M. Ho, "Islanding detection in smart grids," in *Proc. IEEE Energy Convers. Congr. Expo.*, Sep. 2010, pp. 3631–3637.
- [11] R. Teodorescu, M. Liserre, P. Rodriguez, and F. Blaabjerg, *Grid Converters for Photovoltaic and Wind Power Systems*. New York, NY, USA: Wiley, 2011.
- [12] D. Reigosa, F. Briz, C. Blanco, P. García, and J. M. Guerrero, "Active islanding detection using high frequency signal injection," *IEEE Trans. Ind. Appl.*, vol. 48, no. 5, pp. 1588–1597, Sep. 2012.
- [13] D. Reigosa, F. Briz, C. Blanco, P. García, and J. M. Guerrero, "Active islanding detection for multiple parallel-connected inverter-based distributed generators using high frequency signal injection," *IEEE Trans. Power Electron.*, vol. 29, no. 3, pp. 1192–1199, Mar. 2014.
- [14] M. Ciobotaru, R. Teodorescu, P. Rodriguez, A. Timbus, and F. Blaabjerg, "On-line grid impedance estimation for single phase grid-connected systems using PQ variations," in *Proc. IEEE Power Electron. Spec. Conf.*, Jun. 2007, pp. 2306–2312.

- [15] A. V. Timbus, R. Teodorescu, and U. Borup, "Online grid impedance measurement suitable for multiple PV inverters running in parallel," in *Proc. 21st Annu. IEEE Appl. Power Electron. Conf. Expo.*, Mar. 2006, pp. 907–911.
- [16] L. Asiminoaei, R. Teodorescu, F. Blaabjerg, and U. Borup, "A digital controlled PV-inverter with grid impedance estimation for ENS detection," *IEEE Trans. Ind. Appl.*, vol. 20, no. 6, pp. 1480–1490, Nov./Dec. 2005.
- [17] L. Asiminoaei, R. Teodorescu, F. Blaabjerg, and U. Borup, "A new method of on-line grid impedance estimation for PV inverter," in *Proc. 19th Annu. IEEE Appl. Power Electron. Conf. Expo.*, Sep. 2004, pp. 1527–1533.
- [18] M. Ciobotaru, R. Teodorescu, and F. Blaabjerg, "On-line grid impedance estimation based on harmonic injection for grid-connected PV inverter," in *Proc. IEEE Int. Symp. Ind. Electron.*, Jun. 2007, pp. 2473–2442.
- [19] H. Zhao, Q. M. Jonathan Wu, and A. Kawamura, "An accurate approach of nonlinearity compensation for VSI inverter output voltage," *IEEE Trans. Power Electron.*, vol. 19, no. 4, pp. 1029–1036, Jul. 2004.
- [20] S. G. Jeong and M. H. Park, "The analysis and compensation of dead-time effects in PWM inverters," *IEEE Trans. Power Electron.*, vol. 38, no. 2, pp. 108–114, Apr. 1991.
- [21] A. R. Muñoz and T. A. Lipo, "On-line dead-time compensation technique for open-loop PWM-VSI drives," *IEEE Trans. Power Electron.*, vol. 14, no. 4, pp. 683–689, Jul. 1999.
- [22] S.-H. Han, T.-H. Jo, J.-H. Park, H.-G. Kim, T.-W. Chun, and E.-C. Nho, "Dead time compensation for grid-connected PWM inverter," in *Proc. 8th Int. Conf. Power Electron.*, Jun. 2011, pp. 876–881.
- [23] J. L. Lin, "A new approach of dead-time compensation for PWM voltage inverters," *IEEE Trans. Circuits Syst. I, Fundam. Theory Appl.*, vol. 49, no. 4, pp. 476–483, Apr. 2012.
- [24] S. H. Hwan and J. M. Kim, "Dead time compensation method for voltage-fed PWM inverter," *IEEE Trans. Energy Convers.*, vol. 25, no. 1, pp. 1–10, Mar. 2010.
- [25] D. Leggat and R. Kerkman, "Pulse based time compensator for PWM voltage inverters," in *Proc. IEEE IECON 21st Int. Conf. Ind. Electron., Control, Instrum.*, 1995, pp. 474–481.
- [26] T. Sukegawa, K. Mizuno, T. Matsui, and T. Okuyama, "Fully digital, vector controlled PWM VSI-fed AC drives with an inverter dead-time compensation strategy," *IEEE Trans. Ind. Appl.*, vol. 27, no. 3, pp. 552–559, May/June 1995.
- [27] D. Reigosa, F. Briz, M. W. Degner, P. Garcia, and J. M. Guerrero, "Magnet temperature estimation in surface PM machines during six-step operation," *IEEE Trans. Ind. Appl.*, vol. 48, no. 6, pp. 2353–2361, Dec. 2012.
- [28] CNE, "Legislation development of the Spanish Electric Power Act," vol. 4, *Royal Decree 1663/2000*, 2002.
- [29] *IEEE Recommended Practice for Utility Interface of Photovoltaic (PV) Systems*, IEEE Standard 929, 2000.
- [30] *IEC Photovoltaic (PV) Systems. Characteristics of the Utility Interface*, IEC Standard 61727, 2004.
- [31] *Criteria for Connection of Generation Systems to ENEL Low Voltage Distribution Networks*, ENEL DK 5940, 2006.
- [32] F. Briz, D. Reigosa, C. Blanco, and J. M. Guerrero, "Coordinated operation of parallel-connected inverters for active islanding detection using high frequency signal injection," *IEEE Trans. Ind. Appl.*, vol. 50, no. 5, pp. 3476–3484, Sep./Oct. 2014. [Online]. Available: www.mitshubishielectric.com
- [33] G. G. Pozzebon, A. F. Q. Goncalves, G. G. Pena, N. E. M. Mocambique, and R. Q. Machado, "Operation of a three-phase power converter connected to a distribution system," *IEEE Trans. Ind. Electron.*, vol. 60, no. 5, pp. 1810–1818, May 2013.
- [34] J. Muñoz-Cruzado-Alba, J. Villegas-Núñez, J. A. Vite-Frias, J. M. Carrasco-Solis, and E. Galvan-Diez, "New low-distortion Q-F droop plus correlation anti-islanding detection method for power converters in distributed generation systems," *IEEE Trans. Ind. Electron.*, vol. 62, no. 8, pp. 5072–5081, Aug. 2015.
- [35] D. Reigosa, F. Briz, C. Blanco, and J. M. Guerrero, "Islanding detection in three-phase and single-phase systems using pulsating high frequency signal injection," *IEEE Trans. Power Electron.*, vol. 30, no. 12, pp. 6672–6683, Dec. 2015.
- [36] Y. Zhu *et al.*, "A novel RPV (reactive-power-variation) antiislanding method based on adapted reactive power perturbation," *IEEE Trans. Power Electron.*, vol. 28, no. 11, pp. 4998–5012, Nov. 2013.
- [37] A. Yafaoui, B. Wu, and S. Kouro, "Improved active frequency drift anti-islanding detection method for grid connected photovoltaic systems," *IEEE Trans. Power Electron.*, vol. 27, no. 5, pp. 2367–2375, May 2012.
- [38] P. O'Kane and B. Fox, "Loss of mains detection for embedded generation by system impedance monitoring," in *Proc. 6th Int. Conf. Develop. Power Syst. Protection*, Mar. 1997, pp. 95–98.
- [39] N. Liu, A. Aljankawey, C. Diduch, L. Chang, and J. Su, "Passive islanding detection approach based on tracking the frequency-dependent impedance change," *IEEE Trans. Power Del.*, vol. 30, no. 6, pp. 2570–2580, Dec. 2015.
- [40] S. H. Han, T. H. Jo, J. H. Park, H. G. Kim, T. W. Chun, and E. C. Nho, "Dead time compensation for grid-connected PWM inverter," in *Proc. IEEE Int. Conf. Power Electron.*, 2011, pp. 876–881.
- [41] Y. Wang, Q. Gao, and X. Cai, "Mixed PWM for dead-time elimination and compensation in a grid-tied inverter," *IEEE Trans. Ind. Electron.*, vol. 58, no. 10, pp. 4797–4803, Oct. 2011.
- [42] M. A. Herran, J. R. Fischer, S. A. Gonzalez, M. G. Judewicz, and D. O. Carrica, "Adaptive dead-time compensation for grid-connected PWM inverters of single-stage PV systems," *IEEE Trans. Power Electron.*, vol. 28, no. 6, pp. 2816–2825, Jun. 2013.
- [43] N. Urasaki, T. Senjyu, K. Uezato, and T. Funabashi, "An adaptive dead-time compensation strategy for voltage source inverter fed motor drives," *IEEE Trans. Power Electron.*, vol. 20, no. 5, pp. 1150–1160, Sep. 2005.
- [44] D. H. Lee and J. W. Ahn, "A simple and direct dead-time effect compensation scheme in PWM-VSI," *IEEE Trans. Ind. Appl.*, vol. 50, no. 5, pp. 3017–3025, Sep./Oct. 2015.
- [45] H. Wang, X. Pei, Y. Chen, Y. Kang, and X. Yue, "An adaptive dead-time compensation method for sinusoidal PWM-controlled voltage source inverter with output LC filter," in *Proc. 26th Annu. IEEE Appl. Power Electron. Conf. Expo.*, Mar. 2011, pp. 778–785.
- [46] Y. Liu, H. Ben, C. Li, and D. Wang, "Research of the dead-time compensation based on the three-phase grid-connected inverter," in *Proc. 7th Int. Power Electron. Motion Control Conf.*, Jun. 2012, pp. 510–514.
- [47] S.-H. Han, T.-H. Jo, J.-H. Park, H.-G. Kim, T.-W. Chun, and E.-C. Nho, "Dead time compensation for grid-connected PWM inverter," in *Proc. 8th Int. Power Electron.*, Jun. 2011, pp. 876–881.
- [48] T.-K. Vu, B.-M. Han, and H. Cha, "A new adaptive dead-time compensation for single-phase grid-connected PV inverter," in *Proc. 26th Annu. IEEE Appl. Power Electron. Conf. Expo.*, Mar. 2011, pp. 923–930.



David Díaz Reigosa (S'03–M'07) was born in Spain in 1979. He received the M.E. and Ph.D. degrees in electrical engineering from the University of Oviedo, Gijón, Spain, in 2003 and 2007, respectively.

From 2004 to 2008, he was awarded a fellowship of the Personnel Research Training Program funded by the Regional Ministry of Education and Science of the Principality of Asturias. He was a Visitor Scholar at the Wisconsin Electric Machines and Power Electronics Consortium, University of Wisconsin, Madison, in 2007. He was a Visiting Professor at the Electrical Machines and Drives Group, University of Sheffield, in 2016. He is currently an Associated Professor in the Department of Electrical Engineering, University of Oviedo. His research interests include sensorless control of induction motors, permanent magnet synchronous motors, microgrids, distributed generation, and digital signal processing.



Fernando Briz (A'96–M'99–SM'06) received the M.S. and Ph.D. degrees from the University of Oviedo, Gijón, Spain, in 1990 and 1996, respectively.

From June 1996 to March 1997, he was a Visiting Researcher with the University of Wisconsin, Madison, USA. He is currently a Full Professor with the Department of Electrical, Computer, and Systems Engineering, University of Oviedo. His current research interests include control systems, power converters and ac drives, machine diagnostics, and digital signal processing.

Dr. Briz received the 2005 IEEE TRANSACTIONS ON INDUSTRY APPLICATIONS Third Place Prize Paper Award and was the recipient of eight IEEE Industry Applications Society Conference and the IEEE Energy Conversion Congress and Exposition Prize Paper Awards. He is currently the Publications Chair of the Industrial Drives Committee of the Industrial Power Conversion Systems Department of the IEEE Industry Applications Society.



Cristian Blanco Charro (M'11) was born in Spain in 1985. He received the B.S. degree in telecommunications engineering in 2010 and the M.S. and Ph.D. degrees in electrical engineering in 2011 and 2015, respectively, all from the University of Oviedo, Gijón, Spain.

In 2011, he received a fellowship of the Personnel Research Training Program funded by the Regional Ministry of Education and Science of the Principality of Asturias. From September 2012 to February 2013, he was a Ph.D. guest with Aalborg University. He is currently an Assistant Professor with the Department of Electrical, Computer, and Systems Engineering, University of Oviedo. His research interests include modeling and control of islanded and grid-connected converters, synchronization, islanding detection and power quality, microgrids, and digital signal processing.

Dr. Blanco Charro received the IEEE Energy Conversion Congress and Exposition Prize Paper Award in 2012 and the University of Oviedo Outstanding Ph.D. Thesis Award in 2016.



Juan M. Guerrero (S'00–A'01–M'04) received the M.E. degree in industrial engineering and the Ph.D. degree in electrical and electronic engineering from the University of Oviedo, Gijón, Spain, in 1998 and 2003, respectively.

Since 1999, he has occupied different teaching and research positions with the Department of Electrical, Computer and Systems Engineering, University of Oviedo, where he is currently an Associate Professor. From February to October 2002, he was a Visiting Scholar at the University of Wisconsin, Madison.

From June to December 2007, he was a Visiting Professor at the Tennessee Technological University, Cookeville. His research interests include control of electric drives and power converters, smart grids, and renewable energy generation.

Dr. Guerrero received an award from the College of Industrial Engineers of Asturias and León, Spain, for his M.E. thesis in 1999, the IEEE Industry Applications Society Conference Prize Paper Award in 2003, and the University of Oviedo Outstanding Ph.D. Thesis Award in 2004.